Surface & Coatings Technology 205 (2011) S312–S316

Contents lists available at ScienceDirect

Surface & Coatings Technology

journal homepage: www.elsevier.com/locate/surfcoat

Time-resolved plasma characterisation of modulated pulsed power magnetron sputtering of chromium

B. Liebig [a], N. St J. Braithwaite [b], P.J. Kelly [c], R. Chistyakov [d], B. Abraham [d], J.W. Bradley [a,*]

[a] Department of Electrical Engineering and Electronics, University of Liverpool, Brownlow Hill, Liverpool, L69 3GJ, UK
[b] Department of Physics and Astronomy, The Open University, Walton Hall, Milton Keynes, MK7 6AA, UK
[c] Surface Engineering Group, Manchester Metropolitan University, Chester Street, Manchester, M1 5GD, UK
[d] Zpulser, LLC, MA, USA

ARTICLE INFO

Article history:
Received 14 September 2010
Accepted in revised form 10 January 2011
Available online 15 January 2011

Keywords:
Modulated Pulsed Power Magnetron Sputtering
HIPIMS
Langmuir probe
Plasma diagnostic

ABSTRACT

Time-resolved Langmuir probe measurements have been employed to investigate the temporal development of the plasma properties, such as electron and ion density, electron temperature as well as the floating and plasma potential, during Modulated Pulsed Power Magnetron Sputtering (MPPMS). A chromium target was sputtered with an average power of 650 W in an argon atmosphere (0.53 Pa) employing two steps of excitation of the discharge which was realised by altering the modulation frequency of the voltage supplied to the target. The overall pulse duration was kept at 750 μs and a repetition frequency of 100 Hz was used. Three distinct stages of the discharge, namely the initial and the second step of excitation as well as the transition region which connects both stable states, were found. Maximum electron densities up to 7×10^{11} cm^{-3} were obtained during the transient phase.

1. Introduction

High Power Impulse Magnetron Sputtering (HIPIMS or HPPMS) first introduced by Kouznetsov et al. in 1999 [1] utilises short pulses at a low frequency (duty cycle typically <10%) in combination with a high instantaneous power, leading to electron densities higher than 10^{12} cm^{-3} during the pulse [2,3]. The progress made in film deposition and properties, as well as in the investigation of the underlying physics has recently been reviewed by Helmersson et al. [4], Alami et al. [5] and Sarakinos et al. [6]. Despite the large amount of benefits, this technique suffers from a big disadvantage which is the lower deposition rate compared to DC and pulsed DC magnetron sputtering [7–13].

In order to overcome the loss of deposition rate, an alternative technique has been introduced, Modulated Pulse Power Magnetron Sputtering (MPPMS) [14]. This type of power supply makes use of longer pulse widths up to 3 ms at similar repetition rates in the range between several 10 Hz and a few 100 Hz, leading to duty cycles well above 5% (up to 25%). However, the main feature is the superimposition of the so-called macropulse, i.e. the voltage pulse with a duration of up to 3 ms, with shorter micropulses with frequencies in the range of several 10 kHz. The 'on'- and 'off'-time of these micropulses which are typically up to several 10 μs, as well as their frequency can be altered within the macropulses. The result is a rather complex step-like shape of the target voltage and the discharge current waveform. For applications, a stable low density plasma is ignited utilising low micropulse 'on'-times and long 'off'-times. In a second step a high density plasma with power densities of several 100 W cm^{-2} is created by increasing the length of the micropulses' 'on'-time while reducing the 'off'-time [14–16].

Measurements of the ion energy distribution functions and mass spectra while sputtering a chromium target in a nitrogen/argon atmosphere revealed that in addition to ions of nitrogen and argon there is a significant increase in the amount of chromium ions compared to DCMS operated at the same power [17].

However, no investigation of key parameters of the plasma such as the electron density and the electron temperature during MPPMS has yet been published. Therefore, in this study, Langmuir probe measurements were carried out in order to obtain temporally resolved electron density, ion density, electron temperature, floating potential and plasma potential. While keeping the background pressure, the average power, the overall macropulse duration and the initial stage of excitation constant, the influence of the micropulse settings during the second step of excitation was investigated.

2. Experimental

All experiments were carried out in a stainless steel chamber with a diameter of 400 mm and a length of 600 mm, which was pumped down to a base pressure of 2×10^{-4} Pa by a combination of a rotary and a turbo-molecular pump. The cylindrical magnetron V-tech™ 150 from GENCOA Ltd. was mounted at the centre of one of the end flanges

* Corresponding author. Tel.: +44 151 794 4545.
E-mail address: j.w.bradley@liverpool.ac.uk (J.W. Bradley).

0257-8972/$ – see front matter.
doi:10.1016/j.surfcoat.2011.01.017

and equipped with a circular chromium target (purity 99.95%) 150 mm in diameter and 6 mm thick. No substrate was used in any of the measurements presented here. The working gas, research grade argon, entered via a mass flow controller MKS 1179A and the throttle valve was altered to change the pumping speed to maintain a constant pressure of 0.53 Pa (4 mTorr) which was monitored by a Baratron® pressure gauge. A flow rate of 30 sccm argon was used for all experiments. An average power of 650 W (6.5 J per pulse) was supplied to the target by the MPP pulsing unit Zpulser Axia fed by a Pinnacle Plus power supply operated in DC constant voltage mode. The macropulse length was chosen to be 750 μs with a repetition frequency of 100 Hz and consisted of an initial step of excitation (duration 500 μs) with a micropulse 'on'-time of 6 μs and an 'off'-time of 34 μs. During the second step of excitation (250 μs long), the micropulse 'on'-time was kept at 8 μs while the 'off'-time was chosen to be 10 μs. The target voltage and discharge current waveforms were recorded by a Tektronix TDS3014 digital oscilloscope with a 100:1 voltage probe P5100 and a TCP202 current probe in combination with a 20:1 high current transformer CT4 connected.

A schematic diagram of the setup can be found in Fig. 1. The Langmuir probe consisted of a tungsten wire (radius r_p of 0.05 mm) held at one end in an alumina sleeve within which the connection was made to the external circuit. The length of the tungsten wire exposed to the plasma and thus sufficient for collecting the probe current, l_p, was between 3.7 mm and 4.2 mm; the tip was located 10 cm from the target and perpendicular to the local magnetic field (parallel to the target surface). The entire probe head was attached to a stainless steel stem that also served as a feed-through for the electrical wire. An automated acquisition system SmartProbe™ from Scientific Systems Ltd. was used to obtain the current voltage characteristics from the Langmuir probe. The bias voltage V_b was scanned between -95 V and +20 V in steps of $\Delta V_b \approx 0.6$ V and the probe current I_p recorded. During each voltage step, a constant bias was applied to the probe. The current I_p was measured in a time window (width 1 μs, sweeping frequency 1 MHz) triggered by a digital delay generator DG 535 (Stanford Research Systems) which synchronised the measurement with the discharge by introducing an adjustable delay between the target voltage (input) and its TTL output. In this way, about 200 current and voltage data pairs were collected for each voltage scan, building the recorded I_p–V_b-characteristic from an average of five successive scans. For the number densities encountered here one can reasonably expect the space-charge around the Langmuir probe tip to have achieved a quasi-stationary state within temporal resolution of the system (the ion plasma period, $\omega_{pi}^{-1} \ll 1\mu s$). To avoid any influence on the measurements from chromium coatings deposited on the probe tip, the probe was frequently replaced and consistency was checked by comparing I_p–V_b-characteristics recorded in a DC discharge operated in argon (power supply Advanced Energy Pinnacle Plus, $P = 400$ W, $p = 0.53$ Pa).

The I_p–V_b-characteristics obtained were analysed to determine the electron and ion density, as well as the electron temperature and the floating potential and the plasma potential using orbital motion limited theory (OML) [18,19]. OML theory can be used, as the conditions for a collisionless sheath were found to be satisfied, i.e. the mean free paths for electron-neutral and ion-neutral collisions are larger than the Debye length. There are however further criteria for the application of OML to ion collection but the simplicity and directness of the method is such that in this preliminary analysis the OML model will be used without further qualification. The particle densities n can be calculated from the current to the cylindrical probe in the respective saturation regime ($|V_{pl} - V_b| \gg k_B T_x$):

$$I_x = 2\, e\, n_x\, l_p\, r_p \left(\frac{2e\,|V_{pl} - V_b|}{m_x} \right)^{1/2} \tag{1}$$

with the subscript x indicating either ions or electrons as the particles of interest. The electron temperature was estimated from the semi-logarithmic plot of the electron current in the region of the characteristic immediately below plasma potential.

3. Results and discussion

The target voltage V_T and discharge current I_D waveforms for a micropulse 'on'-time of 8 μs and an 'off'-time of 10 μs are shown in Fig. 2. The two step excitation is indicated by the schematic square target voltage waveform (light grey line) as set at the pulsing unit. It can clearly be seen that both the frequency of the micropulses as well as the average value of the target voltage increases from the initial step of excitation to the second one. This is also reflected by the actual measured voltage supplied to the target that reveals a more sawtooth-like form. It is worth noting that only the switching frequency of the micropulses could be

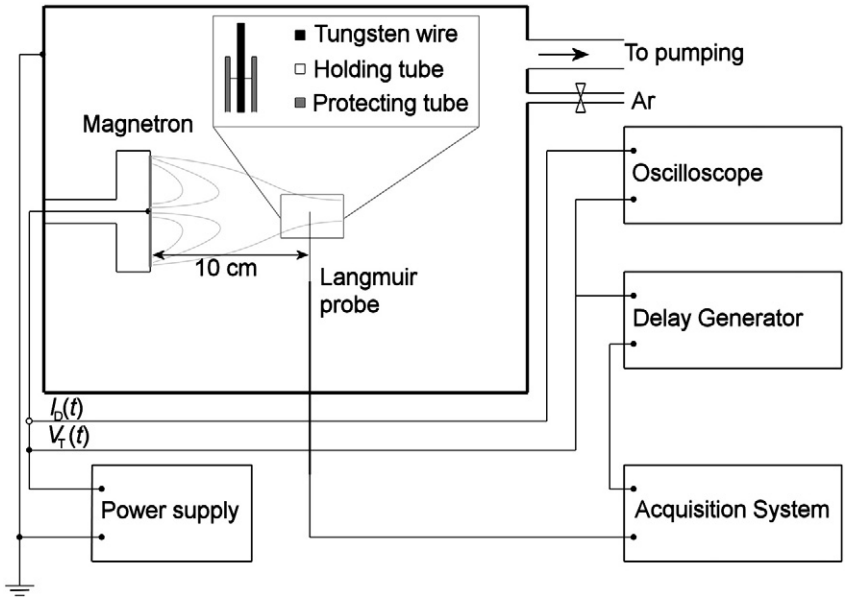

Fig. 1. Schematic drawing of the experimental setup and the design of the Langmuir probe. The target voltage V_T and the discharge current I_D were monitored by an oscilloscope. In addition, the target voltage signal was used to synchronise the measurement with the discharge. Hall probe measurements were carried out to determine the magnetic field geometry of the unbalanced magnetron.

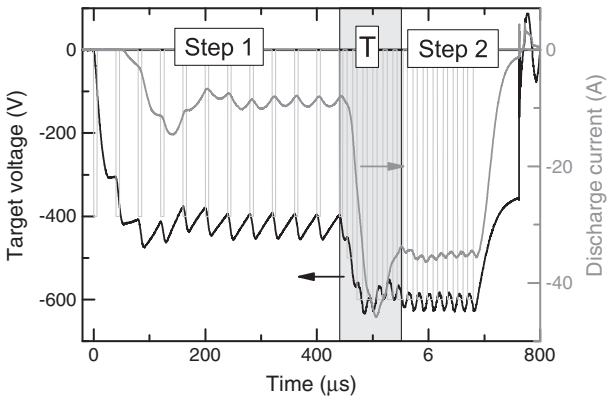

Fig. 2. Target voltage and discharge current waveforms during MPPMS of chromium in an argon atmosphere (0.53 Pa). Two stable stages, steps 1 and 2, as well as a transition region are present. The schematic square waveform (light grey) indicates the programmed 'on'- and 'off'-time of the micropulses.

programmed but not the amplitude of the output voltage. The discharge current follows both voltage ramps, i.e. the pulse initiation and the transition to the second step of excitation, with a delay of a few 10 µs. During stable conditions, an average current of (9.2 ± 0.7) A and (35.2 ± 0.4) A can be reported for the first and the second step of excitation, respectively. Unlike the target voltage, the discharge current reveals a distinct maximum (45.9 A) during the transition between the two stable stages. This suggests, that the increase of the target voltage after about 500 µs, initially leads to a higher ionisation in front of the target and consequently to a higher ion current to the target and enhanced sputtering. However, the resulting high flux of sputtered material may cause rarefaction of the working gas in front of the cathode and its replacement by the sputtered metal vapour [20]. Investigations carried out by Anders et al. with constant target voltages up to 1000 V revealed that a runaway into the self-sustained sputtering mode was not observed for chromium as target material but that there was a maximum in the discharge current as observed in the present experiments, too. The flexibility of the pulsing unit facilitates the use of subsequent pulses with increasing target voltage to keep the discharge in the transition regime. Investigations of this kind, however, are beyond the scope of this paper.

The electron and ion densities (Fig. 3) follow the discharge current also exhibiting the two stable stages of the discharge. The OML analysis of electron and ion saturation regions deduces different densities for electrons and ions, though of course in practice, the plasma bulk must be very closely quasi-neutral; the discrepancy reflects that the conditions of charge collection are less than ideal. Nevertheless the values and the trends are sufficiently close to characterise the plasma behaviour. For the first and the second step of excitation the number density is estimated to be $(1.31 \pm 0.08) \times 10^{11}\,\mathrm{cm}^{-3}$ and $(3.55 \pm 0.08) \times 10^{11}\,\mathrm{cm}^{-3}$ for electrons and $(2.35 \pm 0.13) \times 10^{11}\,\mathrm{cm}^{-3}$ and $(3.92 \pm 0.08) \times 10^{11}\,\mathrm{cm}^{-3}$ for ions. The transition phase is, like the discharge current, characterised by an elevated electron and ion density of $4.5 \times 10^{11}\,\mathrm{cm}^{-3}$ and $4.6 \times 10^{11}\,\mathrm{cm}^{-3}$, respectively. It is worth noting, that both density maxima have a delay of (26 ± 7) µs, averaged over all waveform shapes investigated, in respect to the discharge current peak. Such a phenomenon has been reported previously by Poolcharuansin and Bradley [21], where it was suggested that the travelling time of the sputtered metal flux has to be taken into account. Assuming a similar case here and bearing in mind the probe position being 10 cm in front of the target, a velocity of $(3.9 \pm 1.1)\,\mathrm{km\,s}^{-1}$ can be calculated. This lays indeed in the same range as the drifting velocity of the sputtered metal flux reported by Macák et al. [22] and Hala et al. [23]. After the termination of the pulse, the electron density decreases by three orders of magnitude within the 'off'-time. Two distinct exponential decays can be observed with time constants of (42 ± 8) µs during pulse termination and (840 ± 40) µs about 1 ms after the end of the pulse.

The electron temperature undergoes a more complex development. Two stable stages could also be observed (Fig. 4) with a slight decrease of the electron temperature from (3.50 ± 0.18) eV in the first step of excitation to (2.97 ± 0.07) eV in the second step. As the background gas consists not only of argon but also of a significant fraction of sputtered chromium vapour which has a much lower ionisation threshold (6.77 eV) than argon (15.76 eV), the electron population can maintain ionization and sustain the discharge current with a slightly lower thermal population. During the transient phase, the electron temperature reveals an even lower value of only 2.3 eV at the same temporal position as the electron and ion density maxima occur. This supports the assumption that the sputtered metal flux is arriving at the probe position at this time allowing the electron system to equilibrate at a slightly lower temperature. Another transient phenomenon can be observed during the discharge ignition (first 50 µs), which is the presence of two distinct groups of electrons. In Fig. 4 the extraordinarily high energies exceeding 100 eV obtained from the Langmuir probe I_p–V_b-characteristic within the first 50 µs of the pulse are indicated by the arrows directed towards higher electron temperatures. The voltage transient during the pulse initiation is less than $20\,\mathrm{V\,\mu s}^{-1}$, thus excluding a rapid sheath motion as the origin for these 'super-thermal' electrons, previously observed in HIPIMS discharges by [4,21]. It seems more likely that secondary electrons ejected by ions impinging on the cathode gain energy equal to the target potential in the sheath. As soon as the electron density and the discharge current rise, the fast electrons thermalise rapidly

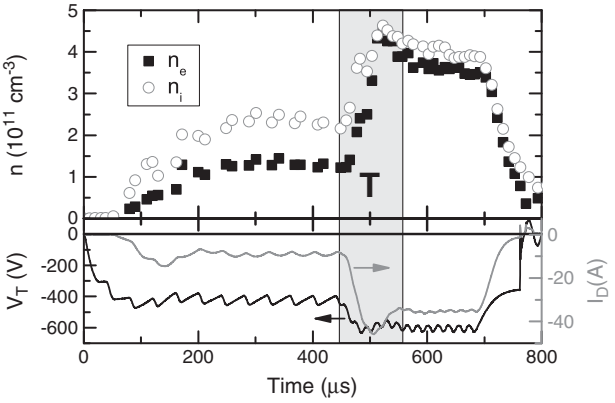

Fig. 3. Temporal development of the electron (black square) and ion density (open circle) during the discharge 'on'-time. Both densities reveal a maximum during the transition stage.

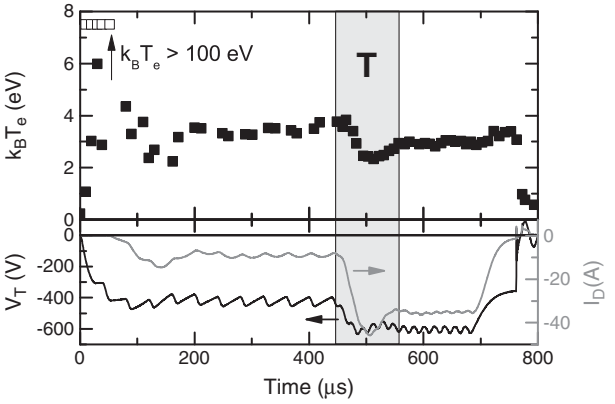

Fig. 4. Temporal development of the electron temperature during the discharge 'on'-time. Electron temperatures exceeding 100 eV during the first 50 µs of the discharge are displayed as open squares with an arrow directing to higher temperatures.

with either the background electrons (via Coulomb interactions) or by inelastic collisions with chromium atoms which originate from the on-set of the sputtering process as suggested by Pajdarová et al. [2], leading to only one group of electrons remaining with a constant temperature as reported above. The presence of two distinct groups of electrons during the initial stage of HIPIMS discharges was reported in [2] and was later confirmed in [21]. However, this phenomenon seems to be related to the nature of pulsed discharges and the voltage ramp during its ignition in particular rather than being typical for HIPIMS, as it has also been observed in pulsed DCMS [24]. Therefore, the current results are consistent with previous studies.

The floating potential V_{fl}, depicted in Fig. 5 can be expected to be displaced from the plasma potential in proportion to the electron temperature, since in a Maxwellian velocity distribution of the electrons can be assumed [25]:

$$V_{fl} - V_p = -\left(\frac{k_B T_e}{2\,e}\right) ln\left(\frac{m_i}{2\pi m_e}\right), \tag{2}$$

with k_B being the Boltzmann constant and m_i and m_e are the ion and the electron mass, respectively. Thus, a constant potential is obtained for both stable stages of the excitation, reflecting the trend in T_e. Interestingly, the transition between these two states is accompanied by subtle changes in the separation of plasma and floating potentials (see Fig. 5 open triangles) beyond the simpler behaviour of T_e during the transition. The results for T_e only show a slight increase which is barely larger than the measuring uncertainty. It can therefore not be confirmed that the electron temperature really increases, but a short period of higher temperature preceding the rise of the current seems plausible in order to create a higher ion density in front of the target leading to the higher discharge current. Finally, the results obtained during pulse initiation (first 50 μs) with floating potentials below the detection limit of −95 V (open squares in Fig. 5) support very well the assumption of very energetic, 'beam-like', electrons during this time. Strongly negative floating potentials during the ignition of the discharge have also been reported by Pajdarová et al. [2] and by Poolcharuansin and Bradley [21].

Fig. 5 also shows the temporal development of the plasma potential within the discharge pulse. After initial transients, steady values of (4.48 ± 0.25) V and (4.05 ± 0.24) V were measured for the first and second step of excitation, respectively. Both the transition and the pulse initiation are characterised by potentials lower than the steady values. As solving the Poisson equation for such a spatially inhomogeneous and time-dependent problem is too complex for this study, a qualitative analysis is presented without any spatial resolution of the plasma itself. The potential drop to the surrounding walls (at potential V_w) can be expressed in terms of electron densities

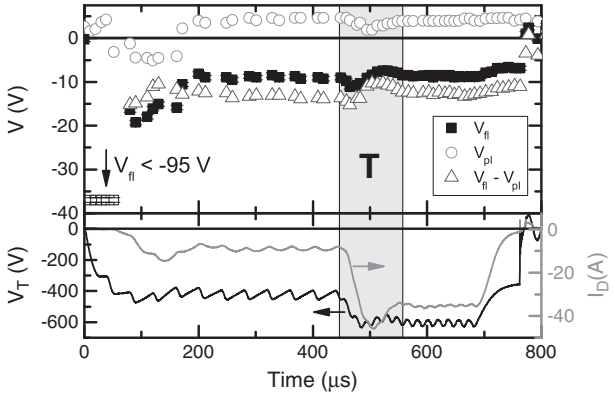

Fig. 5. Temporal development of the floating (black square) and the plasma potential (open circles) during the discharge 'on'-time. Floating potentials below the detection limit of −95 V are indicated by open squares and an arrow directed to lower potentials.

and temperatures at near the cathode and anode by equating the discharge current at the cathode (predominantly an ion current) to that at the anode (predominantly an electron current) [26]:

$$V_{pl} - V_w = \frac{k_B T_e^A}{e} ln\left(\frac{n_e^A A^A}{0.61\, n_i^C A^C}\left(\frac{m_i T_e^A}{2\pi m_e T_e^C}\right)^{1/2}\right), \tag{3}$$

with A being the collecting areas of the cathode and the anode denoted with superscripts C and A, respectively. Of course, the effective areas of the anode (chamber walls) and the cathode are not known, but for a qualitative analysis it can be assumed that both are constant. The chamber walls are grounded $V_w = 0$ V and as an additional assumption T_e^C should be constant as the secondary electrons ejected from the target and accelerated in the sheath lose their energy quite efficiently by elastic collisions with other electrons or inelastic collisions with particles in the gas phase, i.e. argon or chromium. Thus, the plasma potential only depends on the electron density and temperature in front of the chamber walls and the ion density in front of the target. A decrease in the electron temperature during the transition stage may cause the plasma potential to decrease. However, $V_{pl} < 0$ V was obtained for the transition region with different micropulse settings in the second step of excitation (not shown here) and during the pulse initiation as to be seen in Fig. **5**. Thus, the electron temperature alone cannot explain this behaviour, but the ratio between n_e^A and n_i^C has to be investigated. The experimentally obtained electron density may serve as an approximation for n_e^A, while n_i^C can be evaluated from the current flowing to the target, i.e. the discharge current when neglecting secondary electron emission (in practice γ_{see} is unlikely to exceed 0.1). The ion discharge current, carried by ions at the cathode, is given by:

$$I_D = 0.61\, A^C e\, n_i^C \sqrt{\frac{k_B T_e^C}{m_i}}. \tag{4}$$

Since the discharge current is only weakly dependent on T_e^C, an increasing discharge current implies an increased ion density in front of the cathode. As a result of this the ratio n_e^A/n_i^C is expected to decrease and so then does the plasma potential. This allows a higher fraction of the electrons in the plasma volume to escape to the walls (and they may even be ejected from the volume if $V_{pl} < 0$ V) to balance the fluxes of ions and electrons out of the plasma thereby to maintain quasineutrality. Negative plasma potentials during the first half of the pulse of a HIPIMS discharge were also measured with a Langmuir probe by Poolcharuansin and Bradley [21] and with an emissive probe by Mishra et al. [13]. Both studies were carried out under very similar conditions — the size of the chamber and the magnetic field configuration are practically identical though there are differences of target material (Ti in place of Cr) and of power supply. In contrast to this, Pajdarová et al. [2] reported $V_{pl} > 0$ V during the entire discharge pulse, which might be attributed to a different magnetic field configuration. Therefore, different fluxes of charged particles to the chamber walls are expected, which the plasma potential has to balance in order to maintain the quasineutrality of the plasma. However, a general trend might be seen in all these studies: The plasma potential starts with low values and increases during the development of the discharge pulse. An explanation for this phenomenon is given above, considering a global model of the plasma potential.

4. Conclusions

Time-resolved Langmuir probe measurements of a modulated pulsed power magnetron discharge with two step excitation revealed the presence of three distinct stages, namely the two stable stages exhibiting constant values for all plasma parameters and the transition phase which showed an elevated plasma density at a slightly reduced electron temperature. Negative plasma potentials could be

attributed to a temporal imbalance between the ion current towards the cathode and the electron current to the walls, which necessitates the ejection of electrons out of the plasma volume.

Acknowledgement

The work was financially supported by the EPSRC (EP/E003397/1 and EP/E003885/1).

References

[1] V. Kouznetsov, K. Macak, J.M. Schneider, U. Helmersson, I. Petrov, Surf. Coat. Technol. 122 (1999) 290.
[2] A.D. Pajdarová, J. Vlček, P. Kudláček, J. Lukaš, Plasma Sources Sci. Technol. 18 (2009) 025008.
[3] J. Bohlmark, J.T. Gudmundsson, J. Alami, M. Latteman, U. Helmersson, IEEE Trans. Plasma Sci. 33 (2) (2005) 346.
[4] U. Helmersson, M. Lattemann, J. Bohlmark, A.P. Ehiasarian, J.T. Gudmundsson, Thin Solid Films 513 (2006) 1.
[5] J. Alami, S. Bolz, K. Sarakinos, J. Alloy. Comp. 483 (2009) 530.
[6] K. Sarakinos, J. Alami, S. Konstantinidis, Surf. Coat. Technol. 204 (2010) 1661.
[7] J. Alami, K. Sarakinos, G. Mark, M. Wuttig, Appl. Phys. Lett. 89 (15) (2006) 154104.
[8] D.J. Christie, J. Vac. Sci. Technol. A 23 (2005) 330.
[9] S. Konstantinidis, J.P. Dauchot, M. Ganciu, M. Hecq, J. Appl. Phys. 99 (2006) 013307.
[10] J. Emmerich, S. Mráz, R. Snyders, K. Jiang, J.M. Schneider, Vacuum 82 (8) (2008) 867.
[11] J. Vlček, P. Kudláček, K. Burcalová, J. Musil, J. Vac. Sci. Technol. A 25 (2007) 42.
[12] K. Sarakinos, J. Alami, J. Dukwen, J. Wördenweber, M. Wuttig, J. Phys. D Appl. Phys. 41 (2008) 215301.
[13] A. Mishra, P.J. Kelly, J.W. Bradley, Plasma Sources Sci. Technol. 19 (2010) 045014.
[14] W.D. Sproul, R. Chistyakov, B. Abraham, Society of Vacuum Coaters, Summer Bulletin, 2006, p. 35.
[15] R. Chistyakov, B. Abraham, W.D. Sproul, 49th Annual Technical Conference Proceedings of the Society of Vacuum Coaters, 2006, p. 88.
[16] R. Chistyakov, B. Abraham, W.D. Sproul, J. Moore, J. Lin, 50th Annual Technical Conference Proceedings of the Society of Vacuum Coaters, 2007, p. 139.
[17] J. Lin, J.J. Moore, W.D. Sproul, B. Mishra, J.A. Rees, Z. Wu, R. Chistyakov, B. Abraham, Surf. Coat. Technol. 203 (2009) 3676.
[18] H.M. Mott-Smith, I. Langmuir, Phys. Rev. 28 (1926) 727.
[19] F.F. Chen, Phys. Plasmas 8 (2001) 3029.
[20] S.M. Rossnagel, J. Vac. Sci. Technol. A 6 (1) (1988) 19.
[21] P. Poolcharuansin, J.W. Bradley, Plasma Sources Sci. Technol. 19 (2010) 025010.
[22] K. Macák, V. Kouznetsov, J. Schneider, U. Helmersson, I. Petrov, J. Vac. Sci. Technol. A 18 (4) (2000) 1533.
[23] M. Hala, N. Viau, O. Zabeida, J.E. Klemberg-Sapieha, L. Martinu, J. Appl. Phys. 107 (2010) 043305.
[24] J.W. Bradley, H. Bäcker, P.J. Kelly, R.D. Arnell, Surf. Coat. Technol. 135 (2001) 221.
[25] M.A. Lieberman, A.J. Lichtenberg, Principles of Plasma Discharges and Materials Processing, John Wiley & Sons, New York, 1994, chapter 6.
[26] D. Bohm, in: A. Guthrie, R.K. Wakerling (Eds.), The Characteristics of Electrical Discharges in Magnetic Fields, McGraw-Hill, New York, 1949, chapter 3.